From Correspondences to Pose: Non-minimal Certifiably Optimal Relative Pose without Disambiguation

Supplementary Material

In this supplementary material, we provide additional details of our method in Supplementary A, proofs in Supplementaries B and C and experiments in Supplementary D.

A. Additional details

A.1. Averaging of data-dependent constraints

We provide here compact expressions for averaging the data-dependent coefficients of the quadratic terms stemming from Eqs. (22) and (23). We will use the notation $\mathbf{a}^{(j)}$ to refer to the $j-th$ element of a vector $\mathbf{a}$.

Rotation. For clarity, we recall Eq. (22):

$$\bar{\mathbf{f}}_1 \mathbf{E}^\top [\mathbf{t}]_\times \bar{\mathbf{f}}_0 - s_r^2 = 0 \,, \tag{37}$$

The quadratic terms for one correspondence $(\mathbf{f}_0, \mathbf{f}_1)$ are:

$$\begin{aligned}
&\mathbf{f}_0^{(0)}\mathbf{f}_1^{(0)}\mathbf{e}^{(3)}\mathbf{t}^{(2)} + \mathbf{f}_0^{(0)}\mathbf{f}_1^{(1)}\mathbf{e}^{(4)}\mathbf{t}^{(2)} + \mathbf{f}_0^{(0)}\mathbf{f}_1^{(2)}\mathbf{e}^{(5)}\mathbf{t}^{(2)} \\
&+ \mathbf{f}_0^{(1)}\mathbf{f}_1^{(0)}\mathbf{e}^{(6)}\mathbf{t}^{(0)} + \mathbf{f}_0^{(1)}\mathbf{f}_1^{(1)}\mathbf{e}^{(7)}\mathbf{t}^{(0)} + \mathbf{f}_0^{(1)}\mathbf{f}_1^{(2)}\mathbf{e}^{(8)}\mathbf{t}^{(0)} \\
&+ \mathbf{f}_0^{(2)}\mathbf{f}_1^{(0)}\mathbf{e}^{(0)}\mathbf{t}^{(1)} + \mathbf{f}_0^{(2)}\mathbf{f}_1^{(1)}\mathbf{e}^{(1)}\mathbf{t}^{(1)} + \mathbf{f}_0^{(2)}\mathbf{f}_1^{(2)}\mathbf{e}^{(2)}\mathbf{t}^{(1)} \\
&- \mathbf{f}_0^{(0)}\mathbf{f}_1^{(0)}\mathbf{e}^{(6)}\mathbf{t}^{(1)} - \mathbf{f}_0^{(0)}\mathbf{f}_1^{(1)}\mathbf{e}^{(7)}\mathbf{t}^{(1)} - \mathbf{f}_0^{(0)}\mathbf{f}_1^{(2)}\mathbf{e}^{(8)}\mathbf{t}^{(1)} \\
&- \mathbf{f}_0^{(1)}\mathbf{f}_1^{(0)}\mathbf{e}^{(0)}\mathbf{t}^{(2)} - \mathbf{f}_0^{(1)}\mathbf{f}_1^{(1)}\mathbf{e}^{(1)}\mathbf{t}^{(2)} - \mathbf{f}_0^{(1)}\mathbf{f}_1^{(2)}\mathbf{e}^{(2)}\mathbf{t}^{(2)} \\
&- \mathbf{f}_0^{(2)}\mathbf{f}_1^{(0)}\mathbf{e}^{(3)}\mathbf{t}^{(0)} - \mathbf{f}_0^{(2)}\mathbf{f}_1^{(1)}\mathbf{e}^{(4)}\mathbf{t}^{(0)} - \mathbf{f}_0^{(2)}\mathbf{f}_1^{(2)}\mathbf{e}^{(5)}\mathbf{t}^{(0)} \\
&- s_r^2 = 0 \,,
\end{aligned} \tag{38}$$

where, $\mathbf{e} \coloneqq \mathrm{vec}(\mathbf{E}^\top)$, as defined in the main paper.

With this ordering, the coefficients of the first nine terms of Eq. (38) (from $\mathbf{f}_0^{(0)}\mathbf{f}_1^{(0)}$ to $\mathbf{f}_0^{(2)}\mathbf{f}_1^{(2)}$) can be computed as $\mathrm{vec}(\mathbf{f}_1\mathbf{f}_0^\top)$, which is a nine-dimensional vector (one element per coefficient). Thus, the averaging of the terms across n correspondences $\{\mathbf{f}_{0,i}, \mathbf{f}_{1,i}\}_{i=1}^n$ can be expressed as:

$$\mathrm{vec}\left(\frac{1}{n}\sum_{i=1}^{n} \mathbf{f}_{1,i}\mathbf{f}_{0,i}^\top\right) \,. \tag{39}$$

Furthermore, the subsequent nine quadratic terms have the same (but negated) coefficients. Thus, the values of Eq. (39) can be reused for these coefficients.

Translation. For clarity, we recall Eq. (23):

$$h\bar{\mathbf{f}}_0^\top \mathbf{t} - h\bar{\mathbf{f}}_1^\top \mathbf{q} - s_t^2 = 0 \,, \tag{40}$$

The quadratic terms for one correspondence $(\mathbf{f}_0, \mathbf{f}_1)$ are:

$$\begin{aligned}
&h\mathbf{f}_0^{(0)}\mathbf{t}^{(0)} + h\mathbf{f}_0^{(1)}\mathbf{t}^{(1)} + h\mathbf{f}_0^{(2)}\mathbf{t}^{(2)} \\
&-h\mathbf{f}_1^{(0)}\mathbf{q}^{(0)} - h\mathbf{f}_1^{(1)}\mathbf{q}^{(1)} - h\mathbf{f}_1^{(2)}\mathbf{q}^{(2)} \\
&-s_t^2 = 0
\end{aligned} \tag{41}$$

In this case the coefficients of the quadratic terms are directly given by the bearings. Thus, the average for the first three coefficients can be computed as $1/n\sum_i^n \mathbf{f}_0$, and as $-1/n\sum_i^n \mathbf{f}_1$ for the subsequent three coefficients.

A.2. Appropriate scaling of the solution estimates

As explained in Sec. 4.1, we extract the solution estimates from the dominant singular vector, denoted as $\mathbf{v}_0$, of $\mathbf{X}^\star_{\mathbf{E},\mathbf{tq},h} \coloneqq \mathbf{X}^\star_{[1:16,1:16]}$. Following the ordering and notation of the main paper, this corresponds to $\mathbf{v}_0 = [(\mathbf{e}^\star)^\top, (\mathbf{t}^\star)^\top, (\mathbf{q}^\star)^\top, h]^\top$. However, the norm constraints enforced during the optimization, namely $\mathbf{t}^\top\mathbf{t} = 1$, $\mathbf{q}^\top\mathbf{q} = 1$ and $\mathrm{tr}(\mathbf{E}\mathbf{E}^\top) = 2$, apply to $\mathbf{X}^\star$ and not to $\mathbf{v}_0$. Consequently, we cannot assume that the elements of this dominant vector will be scaled appropriately even after multiplying it with its singular value. The solution to this is straightforward: we separately normalize the vectors $\mathbf{t}$ and $\mathbf{q}$ to make them unit vectors, and scale $\mathbf{e} \coloneqq \mathrm{vec}(\mathbf{E}^\top)$ such that its nonzero singular values equal 1 (in practice, we use the SVD of $\mathbf{E}$ for greater precision). Finally, we leverage the absence of products between the slack variable s_t and the rest of the parameters in Prob. (QCQP) to directly read s_t^2 from its corresponding diagonal entry in $\mathbf{X}^\star$, thus avoiding the need to factorize $\mathbf{X}^\star$ to obtain its value.

A.3. Pure rotations and numerical accuracy

Under pure rotations, considering an optimal essential matrix, $\mathbf{E}^\star$, any pair of translation vectors $\mathbf{t}, \mathbf{q} \in \mathcal{S}^2$ satisfying the definition $\mathbf{q} \coloneqq \mathbf{R}^\top\mathbf{t}$ will minimize the sum of squared epipolar errors. Here, $\mathbf{R} \in \mathrm{SO}(3)$ represents one of the two rotation matrices corresponding to $\mathbf{E}^\star$. Given that both $\mathbf{t}, \mathbf{q}$ belong to $\mathcal{S}^2$, one might expect to find two additional singular vectors corresponding to nonzero singular values, in addition to the three singular vectors metioned in Sec. 4.1. However, we empirically verified that four additional singular vectors appear instead. We observed the same phenomenon in [23, 69]. This phenomenon likely occurs because the constraints apply only to the optimal matrix $\mathbf{X}^\star$. Therefore, the elements in the singular vectors of $\mathbf{X}^\star$ do not need to satisfy the norm constraints (*e.g.* that $\mathbf{t}, \mathbf{q}$ belong to $\mathcal{S}^2$) to still minimize the cost function. This may explain the similar behavior noted in [10] regarding pure rotations.

Importantly, in our case, the correct solution can be extracted from the dominant singular vector thanks to Eq. (22), which enforces a larger singular value corresponding to the vector containing the solution. However, for pure rotations and in absence of noise, the component in

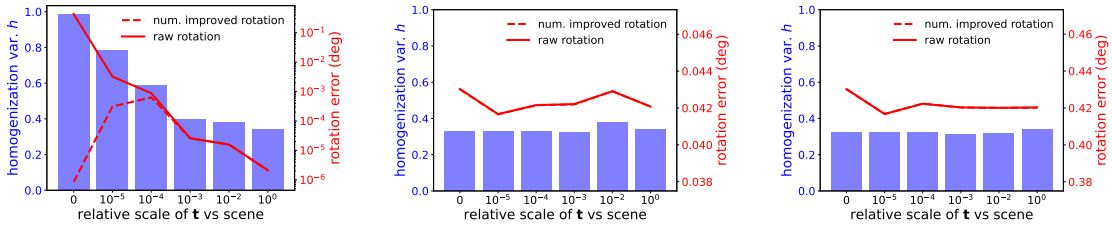

(a) noise = 0 pix (b) noise = 1 pix (c) noise = 10 pix

Figure 8. **Noise-free pure rotation scenarios.** For our method, an edge case consists of noise-free pure rotational motions. In noise-free scenarios (a) the estimate of h within the dominant singular vector—which contains the rest of the solution estimates—approaches 1 in near-pure rotational motions (when the relative scale is $< 10^{-4}$), negatively affecting the numerical accuracy of the other estimates. As can be seen, we effectively address this by using the dominant singular vector from the submatrix excluding h. However, despite the effectiveness of this solution, this numerical issue is not present in practical scenarios (b), (c), where noise affects the observations. These visualizations depict results averaged across 1000 different random instances of the same synthetic scenarios considered in the main paper.

the (unit) singular vector corresponding to the homogenization variable, h, dominates the rest, being close to ~ 1. This predominance reduces the numerical accuracy of the other estimates ($\mathbf{e}, \mathbf{t}$ and $\mathbf{q}$). Since this behavior is only present in a noise-free scenario, we can use a strict threshold in the slack variable s_t^2 (we use 10^{-4}) to detect such scenario. Consequently, only in this case, we extract the solution from the dominant singular vector of the submatrix corresponding only to $\mathbf{e}, \mathbf{t}$ and $\mathbf{q}$, leveraging the previous numerically-inaccurate solution to just correct the sign of this new numerically-accurate solution, if necessary. This behavior is shown in Fig. 8.

B. Tightness of [69] when the SDP solution is rank-2

In [69, Eq. 11] the following QCQP is considered:

Problem QCQP-Z

$$\min_{\mathbf{E},\mathbf{t}} \quad \mathbf{e}^\top \mathbf{C} \mathbf{e} \,, \tag{42}$$

$$\text{s.t.} \quad \mathbf{E}\mathbf{E}^\top = [\mathbf{t}]_\times [\mathbf{t}]_\times^\top, \quad \mathbf{t}^\top \mathbf{t} = 1 \,. \tag{43}$$

The tightness conditions in [69, Th. 2] assume that tightness of the semidefinite relaxation imply $\mathrm{rank}(\mathbf{X}^\star) = 1$, where $\mathbf{X}^\star$ represents the optimal solution of the SDP. In this section, we adapt Theorem 4.1 to extend [69, Th. 2] and show that Prob. (QCQP-Z) can also be tight when $\mathrm{rank}(\mathbf{X}^\star) = 2$.

With a similar notation as in the main paper, let us define the following auxiliary variables:

$$\mathbf{X}_\mathbf{e}^\star := \mathbf{X}^\star_{[1:9,1:9]} \,, \quad \mathbf{X}_\mathbf{t}^\star := \mathbf{X}^\star_{[10:12,10:12]} \,. \tag{44}$$

Theorem B.1. *The semidefinite relaxation of Prob. (QCQP-Z) is tight if and only if* $\mathrm{rank}(\mathbf{X}^\star) \in [1, 2]$*, and its submatrices* $\mathbf{X}_\mathbf{e}^\star$ *and* $\mathbf{X}_\mathbf{t}^\star$ *are rank-1.*

Proof. For the *only if* direction, assume the relaxation is tight. Then, following [10], we can find $\mathbf{X}^\star$ in the convex hull of the linearly independent rank-1 solutions to the relative pose problem[8]:

$$\mathbf{X}^\star := \alpha_0 \mathbf{x}_0 \mathbf{x}_0^\top + \alpha_1 \mathbf{x}_1 \mathbf{x}_1^\top \,, \tag{45}$$

$$\mathbf{x}_0 := \begin{bmatrix} \mathbf{e} \\ \mathbf{t} \end{bmatrix}, \quad \mathbf{x}_1 := \begin{bmatrix} \mathbf{e} \\ -\mathbf{t} \end{bmatrix}, \tag{46}$$

where α_0, α_1 are non-negative scalars such that $\alpha_0 + \alpha_1 = 1$. This last condition ensures that the cost is optimal, *i.e.*, $\mathrm{tr}(\mathbf{C}_0 \mathbf{X}^\star) = \mathbf{e}^\top \mathbf{C} \mathbf{e}$, and that the resulting matrix $\mathbf{X}^\star$ is feasible. To see this, we can expand Eq. (45):

$$\mathbf{X}^\star = \begin{bmatrix} (\alpha_0 + \alpha_1)\mathbf{e}\mathbf{e}^\top & (\alpha_0 - \alpha_1)\mathbf{e}\mathbf{t}^\top \\ (\alpha_0 - \alpha_1)\mathbf{t}\mathbf{e}^\top & (\alpha_0 + \alpha_1)\mathbf{t}\mathbf{t}^\top \end{bmatrix} , \tag{47}$$

to verify that $\alpha_0 + \alpha_1 = 1$ is needed to satisfy the norm constraint $\mathbf{t}^\top \mathbf{t} = 1$ (the rest of the constraints are satisfied for any valid combination of α_0 and α_1). This reveals that when the semidefinite relaxation is tight, the diagonal (upper-left and bottom-right) block matrices are rank-1 and that $\mathrm{rank}(\mathbf{X}^\star) \in \{1, 2\}$. Specifically[9], $\mathrm{rank}(\mathbf{X}^\star) = 1$ when $\alpha_0 = 0$ and $\alpha_1 = 1$ or when $\alpha_0 = 1$ and $\alpha_1 = 0$. Otherwise $\mathrm{rank}(\mathbf{X}^\star) = 2$.

For the *if* part, we build upon [69, Theorem 2]. Since $\mathbf{X}^\star$ is a positive semidefinite (PSD) matrix, $\mathbf{X}_\mathbf{e}^\star$ and $\mathbf{X}_\mathbf{t}^\star$ are also PSD as they are principal submatrices of $\mathbf{X}^\star$ [55]. Given that $\mathbf{X}_\mathbf{e}^\star$ and $\mathbf{X}_\mathbf{t}^\star$ are both rank-1 matrices, it follows that there exist two vectors $\mathbf{e}^\star \in \mathbb{R}^9$ and $\mathbf{t}^\star \in \mathbb{R}^3$ that fulfill the primal problem's constraints and satisfy $\mathbf{e}^\star (\mathbf{e}^\star)^\top = \mathbf{X}_\mathbf{e}^\star$ and $\mathbf{t}^\star (\mathbf{t}^\star)^\top = \mathbf{X}_\mathbf{t}^\star$.

Regarding the rank of $\mathbf{X}^\star$, since it is PSD, it can be factorized as $\mathbf{X}^\star = \mathbf{L}\mathbf{L}^\top$, where $\mathbf{L} \in \mathbb{R}^{12 \times r}$ and $r := \mathrm{rank}(\mathbf{X}^\star)$. Thus, to satisfy the rank-1 property of $\mathbf{X}_\mathbf{e}^\star$ and

[8] Note that the outer products of the negative counterparts, $[-\mathbf{e}^\top, -\mathbf{t}^\top]$ and $[-\mathbf{e}^\top, \mathbf{t}^\top]$, are not included, as they yield the same outer product.

[9] In practice, off-the-shelf SDP solvers [33, 57, 64] return a rank-2 block-diagonal solution [23], which corresponds to setting $\alpha_0 = \alpha_1 = 0.5$ in Eqs. (45) and (47).

$\mathbf{X}_\mathbf{t}^\star$, each column k of $\mathbf{L}$ must be given by: $[a_k\mathbf{e}^\top, b_k\mathbf{t}^\top]^\top$, for some scalars $a_k, b_k \in \mathbb{R}$. This constraint limits the rank of $\mathbf{X}^\star$ to at most 2, as any additional column in $\mathbf{L}$ would be a linear combination of the existing ones. Therefore, since $\mathbf{X}^\star$ must be feasible, this implies that $\text{rank}(\mathbf{X}^\star) \in [1, 2]$ and that it is a convex combination of the two linearly independent solutions, stemming from Eq. (45), and thus the relaxation is tight. □

C. Algebraic derivation of Equation (36)

Given estimates of the relative rotation and translation $(\mathbf{R}, \mathbf{t})$, and a correspondence $(\mathbf{f}_0, \mathbf{f}_1)$, the midpoint method triangulates the corresponding 3D point $\mathbf{p} \in \mathbb{R}^3$. It identifies this point as the midpoint (mean) of the common perpendicular to the two rays originating from the bearings [3]. Specifically, it determines the norms $\lambda_0, \lambda_1 \in \mathbb{R}$ of the 3D points, $\mathbf{p}_0 := \lambda_0\mathbf{f}_0, \mathbf{p}_1 := \lambda_1\mathbf{f}_1$, in each camera reference system, that minimize the squared error $\|\mathbf{p}_0 - (\mathbf{R}\mathbf{p}_1 + \mathbf{t})\|^2$:

$$\lambda_0, \lambda_1 = \arg\min_{\lambda_0,\lambda_1} \|\lambda_0\mathbf{f}_0 - (\lambda_1\mathbf{R}\mathbf{f}_1 + \mathbf{t})\|^2 \,. \tag{48}$$

If the 3D points and their midpoint (mean) satisfy the cheirality constraints, both norms λ_0 and λ_1 will be positive. Otherwise, at least one of the norms will be estimated as negative [60]. As will be shown, it is not necessary to explicitly compute λ_0 and λ_1 to estimate their signs.

The rays of ideal, noise-free correspondences meet in a 3D point, satisfying $\lambda_0\mathbf{f}_0 - \lambda_1\mathbf{R}\mathbf{f}_1 = \mathbf{t}$, or in matrix form:

$$\underbrace{\begin{bmatrix}\mathbf{f}_0 & -\mathbf{R}\mathbf{f}_1\end{bmatrix}}_{\mathbf{A}\in\mathbb{R}^{3\times 2}} \begin{bmatrix}\lambda_0 \\ \lambda_1\end{bmatrix} = \mathbf{t} \tag{49}$$

In practice, we minimize the squared errors. As such, an equivalent solution to Eq. (48) is given as the solution to the system $\mathbf{A}^\top\mathbf{A}\,[\lambda_0,\ \lambda_1]^\top = \mathbf{A}^\top\mathbf{t}$:

$$\begin{bmatrix}1 & -\mathbf{f}_0^\top\mathbf{R}\mathbf{f}_1 \\ -\mathbf{f}_0^\top\mathbf{R}\mathbf{f}_1 & 1\end{bmatrix} \begin{bmatrix}\lambda_0 \\ \lambda_1\end{bmatrix} = \begin{bmatrix}\mathbf{f}_0^\top \\ -(\mathbf{R}\mathbf{f}_1)^\top\end{bmatrix} \mathbf{t} \,, \tag{50}$$

where we have used that $(\mathbf{f}_k)^\top\mathbf{f}_k = 1,\ k \in \{0, 1\}$ since $\mathbf{f}_0,\ \mathbf{f}_1 \in \mathcal{S}^2$. Expanding Equation (50) leads to:

$$\lambda_0 - \lambda_1\mathbf{f}_0^\top\mathbf{R}\mathbf{f}_1 = \mathbf{f}_0^\top\mathbf{t} \,, \tag{51}$$
$$\lambda_1 - \lambda_0\mathbf{f}_0^\top\mathbf{R}\mathbf{f}_1 = -(\mathbf{R}\mathbf{f}_1)^\top\mathbf{t} \,. \tag{52}$$

which leads to the equivalent equations:

$$s^2\lambda_1 = -(\mathbf{R}\mathbf{f}_1)^\top\mathbf{t} + (\mathbf{f}_0^\top\mathbf{R}\mathbf{f}_1)(\mathbf{f}_0^\top\mathbf{t}) \,, \tag{53}$$
$$s^2\lambda_0 = \mathbf{f}_0^\top\mathbf{t} - (\mathbf{f}_0^\top\mathbf{R}\mathbf{f}_1)((\mathbf{R}\mathbf{f}_1)^\top\mathbf{t}) \,. \tag{54}$$

where

$$s^2 := 1 - (\mathbf{f}_0^\top\mathbf{R}\mathbf{f}_1)^2 = \sin^2\angle(\mathbf{f}_0, \mathbf{R}\mathbf{f}_1) \,. \tag{55}$$

Since $s^2 \geq 0$, this implies that the RHS of Eqs. (53) and (54) must be positive for λ_0, λ_1 to be positive too:

$$-(\mathbf{R}\mathbf{f}_1)^\top\mathbf{t} + (\mathbf{f}_0^\top\mathbf{R}\mathbf{f}_1)(\mathbf{f}_0^\top\mathbf{t}) > 0 \,, \tag{56}$$
$$\mathbf{f}_0^\top\mathbf{t} - (\mathbf{f}_0^\top\mathbf{R}\mathbf{f}_1)((\mathbf{R}\mathbf{f}_1)^\top\mathbf{t}) > 0 \,, \tag{57}$$

Lastly, to express Eqs. (56) and (57) in compact form, we can use the property of the cross product:

$$(\mathbf{a}\times\mathbf{b})\cdot(\mathbf{c}\times\mathbf{d}) = (\mathbf{a}\cdot\mathbf{c})(\mathbf{b}\cdot\mathbf{d}) - (\mathbf{a}\cdot\mathbf{d})(\mathbf{b}\cdot\mathbf{c}) \,, \tag{58}$$

for any $\mathbf{a}, \mathbf{b}, \mathbf{c}, \mathbf{d} \in \mathbb{R}^3$, and with $\mathbf{a}\cdot\mathbf{b} = \mathbf{a}^\top\mathbf{b}$ representing the dot product between any vectors $\mathbf{a}, \mathbf{b}$. With this property, we reach the inequalities:

$$(\mathbf{R}\mathbf{f}_1 \times \mathbf{f}_0)\cdot(\mathbf{f}_0 \times \mathbf{t}) > 0 \,, \tag{59}$$
$$(\mathbf{R}\mathbf{f}_1 \times \mathbf{f}_0)\cdot(\mathbf{R}\mathbf{f}_1 \times \mathbf{t}) > 0 \,, \tag{60}$$

corresponding thus to Eq. (36).

D. Additional experiments

D.1. Accuracy vs noise and translation magnitude

In Figure 9, we show additional synthetic experiments. In Fig. 9(a)-(e), we verify that the conclusions drawn in Fig. 6 are consistent across different of levels of noise. In regimes with a small number of points (Fig. 9(a),(c)), our C2P and [23] perform the best. Notably, C2P is faster than [23] (see Fig. 5) and slightly outperforms it in estimating translation (Fig. 9(c)). In regimes with a large number of points, the accuracy of our faster version of C2P is on-par with C2P itself and [23]. In Fig. 9(e), we fix the number of points at 1000 while varying the noise level and observe the same behavior. Finally, in Fig. 9(f), we demonstrate that C2P performs as well as [23, 69] when varying the scale of the translation w.r.t. the scene, and unlike them, C2P is also capable of directly detecting near-pure rotational motions and does not need posterior disambiguation step.

D.2. Real-data

Following [23, 69], we test our method on all the sequences from Strecha et al. [56]. We generate 97 wide-baseline image pairs by grouping adjacent images. For each image pair, correspondences are extracted using DoG + SIFT [43]. We then use the RANSAC implementation of OpenGV [35] to filter out wrong correspondences, setting the inlier threshold to 5 pix, which we found sufficient given the images resolution of 3072×2048 pix. The performance of C2P(-fast) and [23, 69] is shown in Fig. 10. The results align with those from the synthetic experiments. C2P-fast is the fastest among all the methods. However, C2P-fast is not always tight, resulting in a slight loss of accuracy with respect to the alternatives. On the other hand, our C2P is significantly more accurate than [69] and is on-par with [23]. Additionally, our C2P is 40% faster than [23] on average.

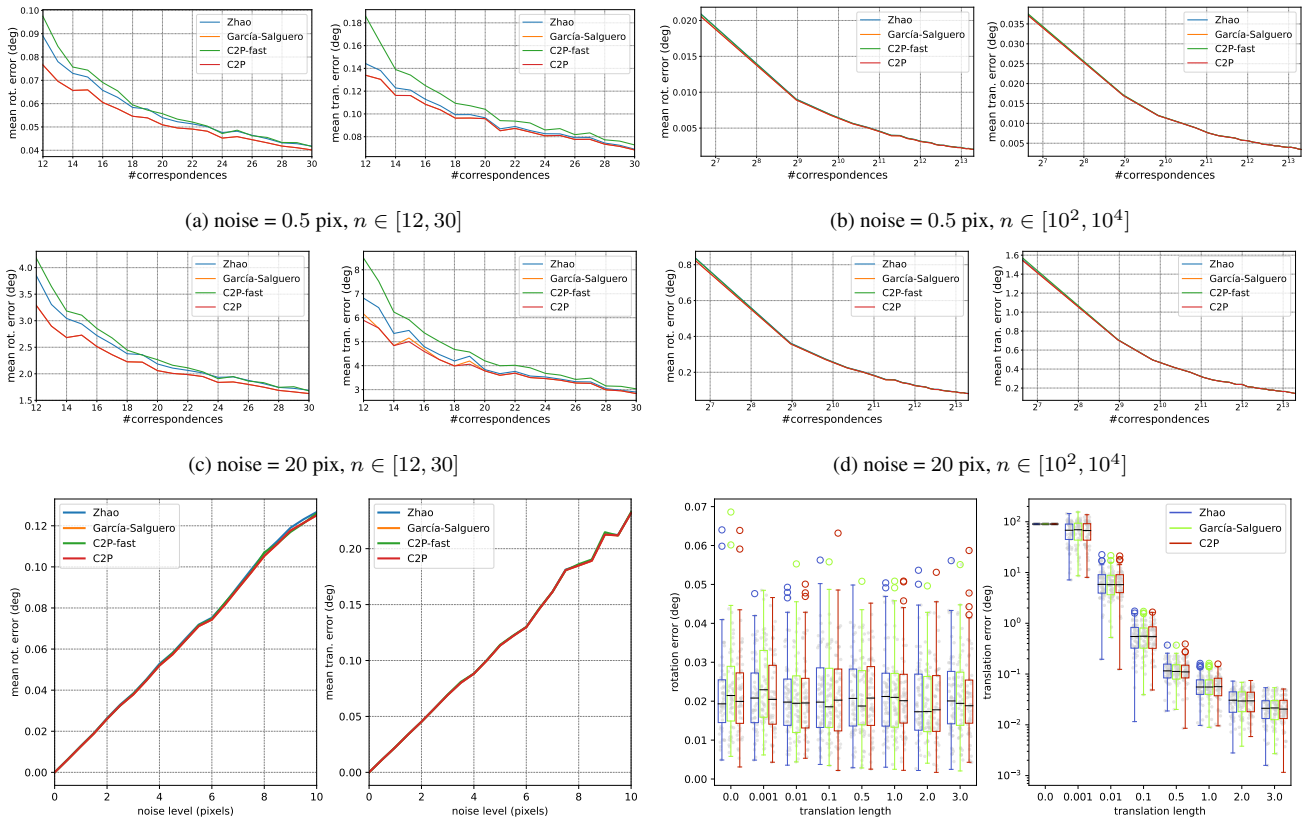

(a) noise = 0.5 pix, $n \in [12, 30]$

(b) noise = 0.5 pix, $n \in [10^2, 10^4]$

(c) noise = 20 pix, $n \in [12, 30]$

(d) noise = 20 pix, $n \in [10^2, 10^4]$

(e) accuracy vs noise level and $n = 1000$

(f) accuracy vs translation length

Figure 9. **Additional synthetic experiments.** We evaluate our proposed C2P and C2P-fast under various conditions: (a)-(d) number of correspondences, (a)-(e) noise levels, and (f) relative translation scale w.r.t. scene. As shown in (b) and (d), C2P-fast is well-suited for scenarios where $n > 10^3$, performing on-par with C2P and [23, 69], while being faster (Fig. 5). With fewer correspondences, as shown in (a) and (c), C2P outperforms [69], slightly surpassing the accuracy of [23] in estimating the translation, while also being faster. The same conclusions are reached when varying the noise levels (e). Finally, in (f) we show that C2P performs as well as [23, 69] when varying the scale of the translation relative to the scene, and unlike them, C2P is capable of directly detecting near-pure rotational motions.

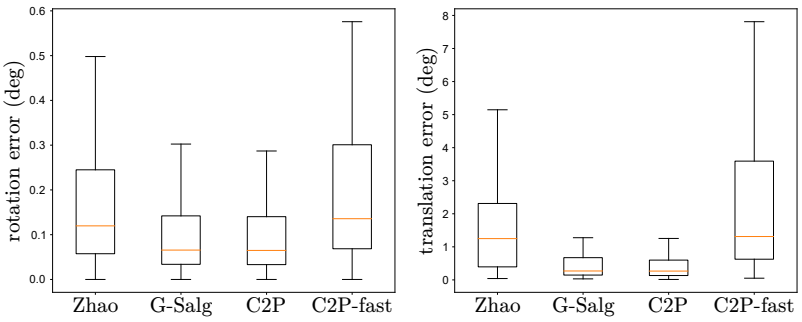

Method	Time (ms)
Zhao [69]	9.2
Garcia-Salguero et al. [23]	14.9
C2P (ours)	10.7
C2P-fast (ours)	9.0

Figure 10. **Performance across all sequences (97 pairs) from Strecha et al. [56].** (left) Relative rotation and translation errors (in degrees) for all image pairs. (right) Averaged execution times for computing the relative pose for each method. As can be seen, C2P-fast is the fastest among all methods. However, C2P-fast is not always tight, resulting in a slight loss of accuracy when compared to the alternatives. On the other hand, our C2P is significantly more accurate than Zhao [69] and is on-par with Garcia-Salguero et al. [23] (labeled on the left as G-Salg.). Additionally, our C2P is, on average, 40% faster than [23].